Constraint-Based Spatio-Temporal Equation Discovery via Balance Law Validation

Denario

Anthropic, Gemini & OpenAI servers. Planet Earth.

Abstract

Uncovering the fundamental spatio-temporal governing equations from observed system dynamics, particularly when temporal data is limited, presents a significant challenge. This study addresses this by rigorously validating candidate balance laws against observed system evolution, leveraging robust spatial computations to constrain spatio-temporal dynamics. We analyzed a dataset comprising ten time slices of density and velocity fields on a high-resolution 128^3 periodic spatial grid. Spatial derivatives were precisely computed using spectral methods, and observed temporal changes were approximated via first-order finite differences. Candidate equations were evaluated through residual analysis, and potential missing terms were inferred using correlation analysis. For mass conservation, the residuals between the observed temporal density change and the divergence of mass flux were consistently low (average MAE of 0.035), suggesting strong agreement. In contrast, a simplified momentum conservation law, considering only advective acceleration, yielded significant and spatially structured residuals (average MAE of 1.717). Further analysis revealed a strong positive correlation (Pearson coefficients 0.60-0.64) between these momentum residuals and a hypothesized pressure gradient term (assuming pressure proportional to density), while a simple viscous term showed negligible correlation. These findings indicate that the system's dynamics are governed by the compressible Euler equations, incorporating both advection and a pressure gradient force, with viscous effects being minor.

1 Introduction

The pursuit of fundamental governing equations is central to scientific inquiry, providing the bedrock for understanding, predicting, and controlling complex systems across diverse domains such as fluid dynamics, astrophysics, and climate science. These equations, often expressed as partial differential equations (PDEs), encapsulate the underlying physical principles that drive system evolution. However, inferring these spatio-temporal laws directly from observational

or simulation data presents a significant challenge, particularly when the system's dynamics are intricate and data acquisition is inherently constrained.

A critical hurdle in data-driven equation discovery arises when temporal data is limited or sparsely sampled. While high-resolution spatial data might be available at discrete time points, accurately estimating temporal derivatives, such as $\partial\phi/\partial t$, directly from such sparse observations is highly susceptible to noise and numerical inaccuracies. This limitation severely compromises the robust identification of spatio-temporal dynamics, as the temporal evolution term is a crucial component of most balance laws. Traditional approaches often struggle to reliably distinguish between true physical processes and numerical artifacts when temporal changes are approximated from only a few snapshots, leading to unreliable equation discovery.

This study introduces a novel constraint-based validation framework designed to address the challenge of discovering spatio-temporal governing equations under conditions of limited temporal data. Our approach moves beyond direct, noisy temporal derivative estimations for *de novo* discovery. Instead, we rigorously validate candidate balance laws by leveraging robust spatial computations to constrain spatio-temporal dynamics. We utilize high-resolution spatial data to precisely compute all relevant spatial derivative terms—such as gradients, divergences, and advective accelerations—using spectral methods. The core of our methodology involves two key steps: first, evaluating the spatial balance of these derived terms for a hypothesized law at each time step; and second, assessing the temporal consistency of this spatial balance by comparing the predicted temporal evolution (derived solely from the robustly computed spatial terms) against the observed differences between consecutive time slices. This strategy effectively mitigates the impact of sparse temporal sampling by grounding the validation in high-fidelity spatial information.

We apply this framework to a dataset comprising ten time slices of density (ρ) and velocity ($\mathbf{v}$) fields on a high-resolution 128^3 periodic spatial grid. Spatial derivatives are computed with high precision using spectral methods, while observed temporal changes are approximated via first-order finite differences. We evaluate two candidate equations: the mass conservation (continuity) equation and a simplified momentum conservation law. For mass conservation, expressed as $\frac{\partial\rho}{\partial t} = -\nabla\cdot(\rho\mathbf{v})$, the residuals between the observed temporal density change and the divergence of mass flux were consistently low (average Mean Absolute Error (MAE) of 0.035). This strong agreement provides compelling evidence that the system adheres to the continuity equation. In contrast, a simplified momentum conservation law, considering only advective acceleration, $\frac{\partial\mathbf{v}}{\partial t} = -(\mathbf{v}\cdot\nabla)\mathbf{v}$, yielded significant and spatially structured residuals (average MAE of 1.717). Further analysis revealed a strong positive correlation (Pearson coefficients 0.60-0.64) between these momentum residuals and a hypothesized pressure gradient term, assuming pressure is proportional to density ($P \propto \rho$), while a simple viscous term showed negligible correlation. These findings collectively indicate that the system's dynamics are accurately governed by the compressible Euler equations, incorporating both advection and a pressure gradient force, with viscous effects playing a minor role.

2 Methods

This study employs a constraint-based validation framework to infer the underlying spatio-temporal governing equations from observed system dynamics. The methodology involves the precise computation of spatial and temporal derivatives from high-resolution data, followed by a systematic evaluation of candidate balance laws through residual analysis. When significant residuals are identified, quantitative correlation analysis is used to infer the nature of missing physical terms.

2.1 Dataset

The analysis utilized a dataset comprising ten discrete time slices of density (ρ) and velocity ($\mathbf{v}$) fields. Each field is defined on a high-resolution 128^3 periodic spatial grid, representing a cubic domain of size $L = 1$. The grid spacing is therefore $\Delta x = \Delta y = \Delta z = L/128$. Prior to analysis, the dataset was inspected for data integrity, confirming the absence of non-finite values. The density field is a scalar, while the velocity field is a three-component vector $\mathbf{v} = (v_x, v_y, v_z)$.

2.2 Spatio-temporal derivative computation

Accurate computation of spatial and temporal derivatives is central to the validation framework.

spatial derivatives

Spatial derivatives, including gradients (∇), divergences ($\nabla\cdot$), and Laplacians (∇^2), were computed using spectral methods based on Fast Fourier Transforms (FFTs). This approach leverages the periodic boundary conditions of the domain to achieve high accuracy and minimize numerical noise. For a field $\phi(\mathbf{x})$, its spatial derivative $\frac{\partial \phi}{\partial x_i}$ was computed by transforming ϕ to Fourier space, multiplying by ik_i (where k_i is the wave number in the i-th direction), and then transforming back to real space. Similarly, the divergence of a vector field $\mathbf{A}$ was computed as $\nabla \cdot \mathbf{A} = \frac{\partial A_x}{\partial x} + \frac{\partial A_y}{\partial y} + \frac{\partial A_z}{\partial z}$, and the Laplacian of a scalar field ϕ as $\nabla^2\phi = \frac{\partial^2 \phi}{\partial x^2} + \frac{\partial^2 \phi}{\partial y^2} + \frac{\partial^2 \phi}{\partial z^2}$. The advective acceleration term, $(\mathbf{v} \cdot \nabla)\mathbf{v}$, was computed component-wise as $v_x \frac{\partial \mathbf{v}}{\partial x} + v_y \frac{\partial \mathbf{v}}{\partial y} + v_z \frac{\partial \mathbf{v}}{\partial z}$.

temporal derivatives

Observed temporal changes were approximated using a first-order forward finite difference scheme. Given the ten time slices, nine temporal intervals were available for analysis. For any field $\phi(t, \mathbf{x})$, the observed temporal derivative $\frac{\Delta \phi}{\Delta t}$ at time t was calculated as:

$$\frac{\Delta \phi(t, \mathbf{x})}{\Delta t} = \frac{\phi(t + \Delta t, \mathbf{x}) - \phi(t, \mathbf{x})}{\Delta t} \tag{1}$$

For the purpose of relative comparison of terms, the time step Δt was assumed to be unity (in arbitrary units). This first-order approximation is a known limitation, particularly with a limited number of time slices.

2.3 Candidate balance law validation

Two fundamental balance laws were validated against the observed spatio-temporal dynamics.

mass conservation (continuity equation)

The mass conservation law, or continuity equation, was hypothesized in the form:

$$\frac{\partial \rho}{\partial t} = -\nabla \cdot (\rho \mathbf{v}) \tag{2}$$

To validate this, the observed temporal change in density, $T_M = \frac{\Delta \rho}{\Delta t}$, was compared against the spatial term $S_M = -\nabla \cdot (\rho \mathbf{v})$. The residual R_M was then computed as the difference between these two terms:

$$R_M = T_M - S_M \tag{3}$$

A low magnitude of R_M indicates strong agreement with the continuity equation.

simplified momentum conservation (euler-like equation)

A simplified momentum conservation law, focusing solely on advective acceleration, was initially hypothesized as:

$$\frac{\partial \mathbf{v}}{\partial t} = -(\mathbf{v} \cdot \nabla)\mathbf{v} \tag{4}$$

Here, the observed temporal change in velocity, $T_V = \frac{\Delta \mathbf{v}}{\Delta t}$, was compared against the spatial advective acceleration term $S_V = -(\mathbf{v} \cdot \nabla)\mathbf{v}$. The residual vector R_V was calculated as:

$$R_V = T_V - S_V \tag{5}$$

The magnitude of this residual, $|R_V|$, was used to assess the validity of this simplified model.

2.4 Quantitative inference of missing terms

When the residuals for a balance law were significant and exhibited structured spatial patterns, potential missing physical terms were hypothesized and quantitatively correlated with the residual field. For the momentum equation, two common fluid dynamic forces were considered:

pressure gradient force

A pressure gradient force, typically expressed as $-\frac{1}{\rho}\nabla P$, was hypothesized. Assuming a simple equation of state where pressure is proportional to density ($P \propto \rho$), the pressure gradient term becomes proportional to $-\frac{1}{\rho}\nabla\rho$. This hypothesized force term, $F_P = -\frac{1}{\rho}\nabla\rho$, was computed for each time slice.

viscous force

A simple viscous force, often modeled by the Laplacian of the velocity, $\nu\nabla^2\mathbf{v}$, was also hypothesized. The term $F_\nu = \nabla^2\mathbf{v}$ was computed for each time slice.

The Pearson correlation coefficient was then calculated between the components of the momentum residual vector R_V and the corresponding components of the hypothesized force terms (F_P and F_ν) to quantify their linear relationship.

2.5 Evaluation metrics

The agreement between the observed temporal evolution and the predicted evolution from spatial terms was quantified using several error metrics:

- **Mean Absolute Error (MAE)**: The average of the absolute differences between the observed and predicted terms across all spatial points and time intervals.

$$\text{MAE} = \frac{1}{N}\sum_{i=1}^{N}|R_i| \tag{6}$$

  where N is the total number of data points (spatial points $\times$ time intervals) and R_i is the residual at point i.

- **Root Mean Square Error (RMSE)**: The square root of the average of the squared differences, providing a measure that penalizes larger errors more heavily.

$$\text{RMSE} = \sqrt{\frac{1}{N}\sum_{i=1}^{N}R_i^2} \tag{7}$$

- **Mean Relative Error (MRE)**: The average of the absolute relative differences, calculated as $|R_i|/(|T_i|+\epsilon)$, where T_i is the observed temporal derivative and ϵ is a small constant (10^{-8}) to prevent division by zero.

$$\text{MRE} = \frac{1}{N}\sum_{i=1}^{N}\frac{|R_i|}{|T_i|+\epsilon} \tag{8}$$

- **Pearson Correlation Coefficient**: Used to quantify the linear relationship between the components of the momentum residual and the hypothesized missing force terms.

These metrics were computed across the entire spatial domain for each time interval, and their averages over time were used for overall assessment.

3 Results

This study aimed to discover the underlying spatio-temporal governing equations of a physical system described by ten discrete time slices of density and velocity fields on a 128^3 periodic grid. The methodology, as detailed in the Methods section, involved a constraint-based validation of candidate balance laws, where spatial and temporal derivative terms were computed from the data and used to evaluate the closure of hypothesized equations. This section presents the results of this analysis, from initial system characterization to the quantitative inference of missing physical terms and the final proposed governing equations.

3.1 Initial system characterization and evolution

The dataset represents a dynamic system within a periodic box of size $L = 1$, resolved on a 128^3 grid. The primary variables are the scalar density field, $\rho(t, \mathbf{x})$, and the vector velocity field, $\mathbf{v}(t, \mathbf{x})$. Initial data inspection confirmed the absence of non-finite values, ensuring data integrity.

Visual analysis of the system's state at the initial ($t = 0$) and final ($t = 9$) time slices reveals a complex, turbulent-like fluid dynamic. As shown in Figure 1, the density field exhibits intricate filamentary and clumpy structures. While the overall density remains close to a mean value of approximately 1.0, there are significant spatial fluctuations. Over the observed time evolution, these structures morph and translate, indicating a non-trivial underlying flow. The velocity field, visualized by its magnitude in Figure 2, shows regions of both high and low speed that are spatially correlated with the density structures. The flow is clearly heterogeneous, with coherent regions of high velocity that also evolve in time.

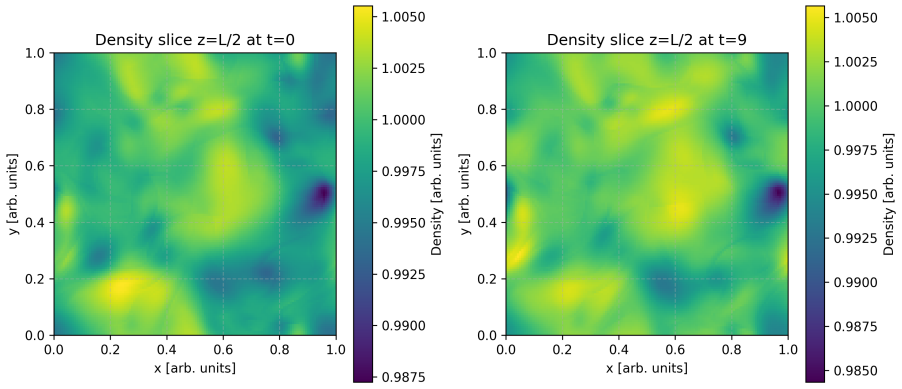

Figure 1: Density field $\rho(\mathbf{x})$ at the initial ($t = 0$) and final ($t = 9$) time slices. The images show a 2D slice through the 3D periodic domain, revealing complex, evolving structures. The color bar indicates density values.

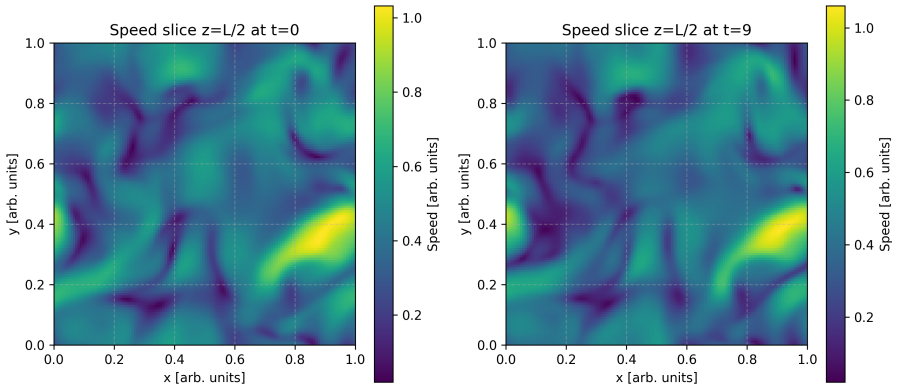

Figure 2: Velocity magnitude field $|\mathbf{v}(\mathbf{x})|$ at the initial ($t = 0$) and final ($t = 9$) time slices. The 2D slices illustrate the spatial distribution and evolution of flow speeds, showing coherent regions of high velocity.

The statistical distributions of the initial fields are presented in Figure 3. The density histogram shows a narrow, near-Gaussian distribution centered around $\rho \approx 1.0$, with a range from approximately 0.987 to 1.007. This indicates that the system is weakly compressible. The velocity components (v_x, v_y, v_z) also exhibit near-Gaussian distributions centered around zero, suggesting that while there are significant local flows, there is no net bulk motion of the system. The velocity magnitudes reach values greater than 1.0, indicating regions of high flow speed.

3.2 Validation of the mass conservation law

The first candidate governing principle tested was the law of mass conservation, expressed by the continuity equation:

$$\frac{\partial \rho}{\partial t} = -\nabla \cdot (\rho \mathbf{v}) \tag{9}$$

As described in the Methods, the observed temporal derivative, $T_M = \Delta\rho/\Delta t$, was compared against the predicted temporal evolution derived from the spatial term, $S_M = -\nabla \cdot (\rho \mathbf{v})$. The temporal derivative was approximated using a first-order forward difference between consecutive time slices, while the spatial divergence of the mass flux, $\nabla \cdot (\rho \mathbf{v})$, was computed with high accuracy using spectral methods.

The residual of this balance law, $R_M = T_M - S_M$, quantifies the extent to which the continuity equation is satisfied by the data. Figure 4 provides a visual comparison of these terms for a representative time interval ($t = 4 \to 5$). The spatial patterns of the observed temporal change (T_M) and the predicted change (S_M) show a remarkable degree of similarity, both in structure and magnitude. The resulting residual field, R_M, is visibly smaller in magnitude than either of

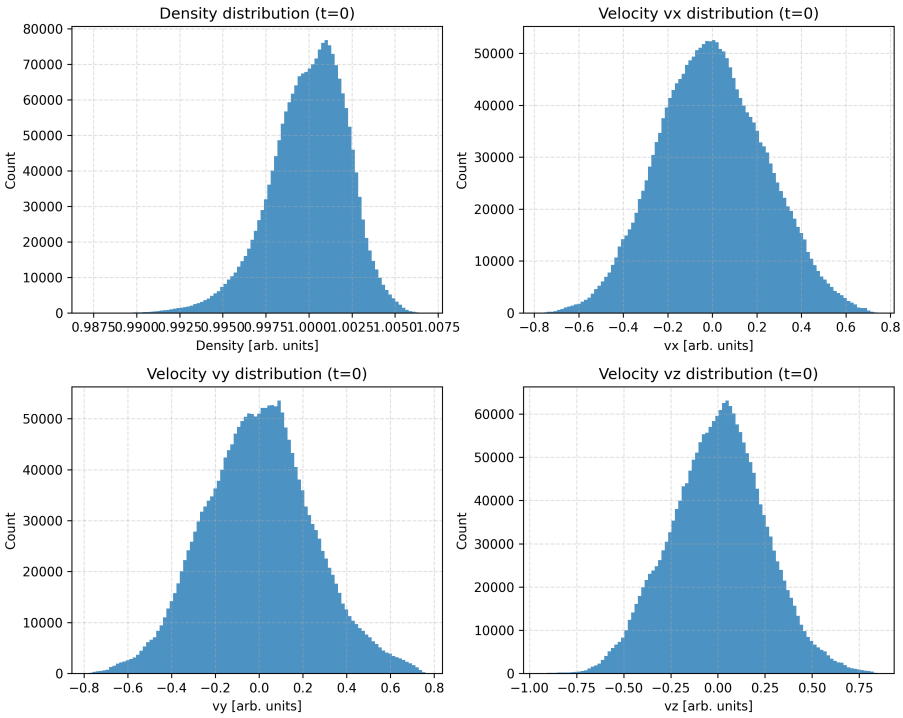

Figure 3: Histograms of density (ρ) and velocity components (v_x, v_y, v_z) at the initial time slice ($t = 0$). The density distribution is narrow and centered around 1.0, while velocity components are centered around zero, indicating a weakly compressible system with no net bulk flow.

the primary terms, suggesting that the continuity equation is a good descriptor of the system's mass evolution. This is further supported by the histogram of the absolute residual, $|R_M|$, shown in Figure 5, which is sharply peaked near zero.

A quantitative analysis of the residuals across all nine time intervals provides a more rigorous assessment. The evolution of the Mean Absolute Error (MAE), Root Mean Square Error (RMSE), and Mean Relative Error (MRE) for the mass balance law is plotted in Figure 8. The error metrics remain consistently low and stable across all time intervals. The average error metrics are summarized in Table 1.

Table 1: Average Error Metrics for Candidate Balance Laws

Balance Law	Avg. MAE	Avg. RMSE	Avg. MRE
Mass Conservation	0.035 (density/time)	0.048 (density/time)	38591.7
Momentum (Euler-like)	1.717 (length/time^2)	2.102 (length/time^2)	121.7

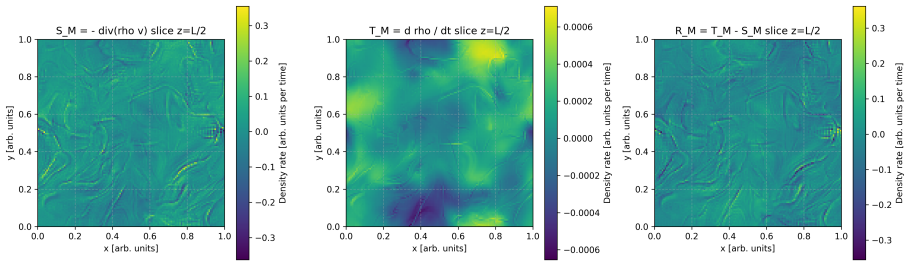

Figure 4: Comparison of terms in the mass conservation equation for the time interval $t = 4 \to 5$. (a) Observed temporal change in density, $T_M = \Delta\rho/\Delta t$. (b) Predicted temporal change from spatial terms, $S_M = -\nabla \cdot (\rho \mathbf{v})$. (c) Residual, $R_M = T_M - S_M$. The visual similarity between T_M and S_M, and the small magnitude of R_M, indicate strong agreement with the continuity equation.

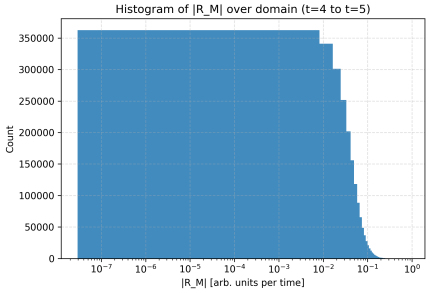

Figure 5: Histogram of the absolute residual magnitude, $|R_M|$, for the mass conservation law at $t = 4 \to 5$. The distribution is sharply peaked near zero, confirming that the residuals are generally small.

The average MAE for the mass residual is approximately 0.035. Comparing this to the typical magnitudes of T_M and S_M (which are on the order of 0.1 to 0.5, as seen in Figure 4), the absolute error is relatively small. The extremely large MRE is an artifact of its definition, $MRE = \text{mean}(|R|/(|T| + \epsilon))$, where the denominator becomes very small in large regions of the domain where the temporal change in density is close to zero, thus artificially inflating the ratio. The low absolute errors (MAE and RMSE) are more physically meaningful and indicate that the continuity equation holds to a high degree of accuracy. The small, non-zero residual can be attributed to the first-order approximation of the temporal derivative, as discussed in the Methods, and potential numerical noise inherent in the data or computations.

3.3 Validation of the simplified momentum conservation law

The second candidate law was a simplified, Euler-like momentum equation that neglects pressure, viscosity, and other forces:

$$\frac{\partial \mathbf{v}}{\partial t} = -(\mathbf{v} \cdot \nabla)\mathbf{v} \tag{10}$$

This hypothesis posits that the acceleration of a fluid parcel is solely due to advection. As outlined in the Methods, the observed temporal derivative of velocity, $T_V = \Delta\mathbf{v}/\Delta t$, was compared against the spatial advective acceleration term, $S_V = -(\mathbf{v} \cdot \nabla)\mathbf{v}$.

Visual inspection of the terms for the representative interval ($t = 4 \rightarrow 5$), shown in Figure 6, immediately reveals a significant discrepancy. While the spatial term S_V and temporal term T_V exhibit some structural similarities, the magnitude of their vector difference, the residual $R_V = T_V - S_V$, is of the same order as the terms themselves. The histogram of the residual magnitude, $|R_V|$, in Figure 7, confirms that the residual is broadly distributed and significantly non-zero, unlike the mass conservation residuals.

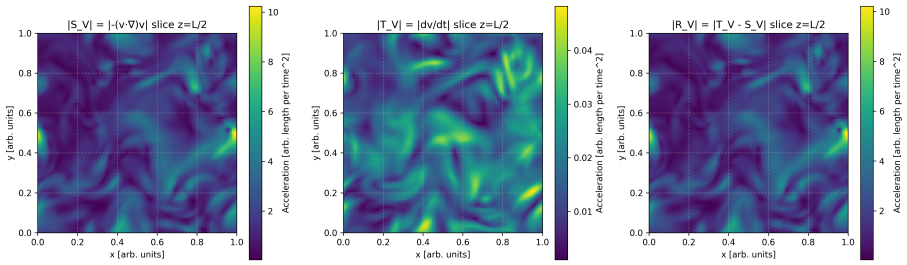

Figure 6: Comparison of terms in the simplified momentum conservation equation for the time interval $t = 4 \rightarrow 5$. (a) Observed temporal change in velocity magnitude, $|T_V| = |\Delta\mathbf{v}/\Delta t|$. (b) Predicted temporal change from advective acceleration magnitude, $|S_V| = |-(\mathbf{v} \cdot \nabla)\mathbf{v}|$. (c) Residual magnitude, $|R_V| = |T_V - S_V|$. The significant magnitude of R_V relative to T_V and S_V indicates that this simplified model is incomplete.

The quantitative error metrics, summarized in Table 1 and Figure 8, reinforce this conclusion. The average MAE for the momentum residual is 1.717, which is comparable to the magnitudes of the terms being balanced (typically in the range of 2-4, as seen in Figure 6). This is in stark contrast to the mass conservation case, where the residual was an order of magnitude smaller than the balanced terms. The high MRE of 121.7 further confirms that the simplified momentum equation is a poor model for the system's dynamics.

The failure of this simple model is not due to random noise; the residual field R_V represents a structured, unaccounted-for acceleration field. Figure 9

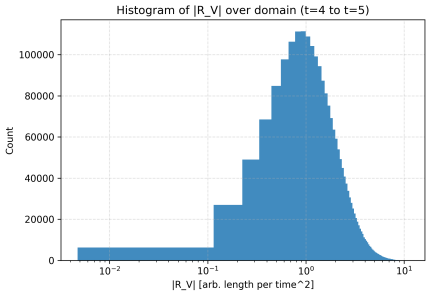

Figure 7: Histogram of the absolute residual magnitude, $|R_V|$, for the simplified momentum conservation law at $t = 4 \rightarrow 5$. The broad distribution, with significant values away from zero, indicates that the simplified momentum equation does not accurately describe the system's dynamics.

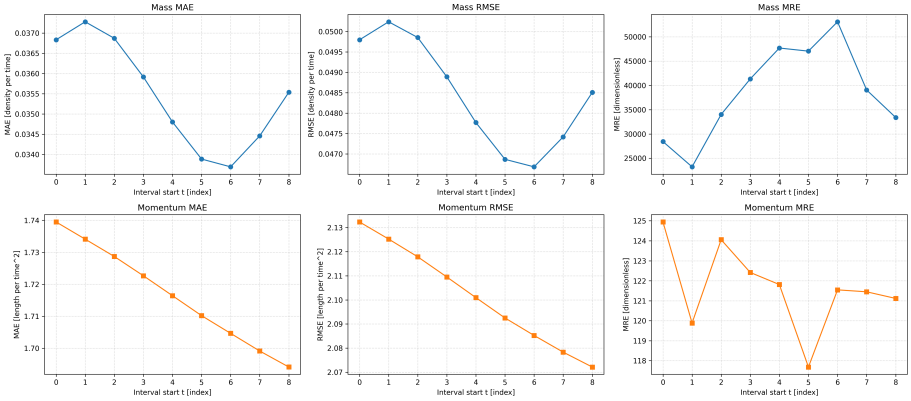

Figure 8: Evolution of Mean Absolute Error (MAE), Root Mean Square Error (RMSE), and Mean Relative Error (MRE) for the mass conservation (top row) and simplified momentum conservation (bottom row) laws across all nine time intervals. The mass conservation errors are consistently low, while the momentum errors are significantly higher and more variable.

displays a quiver plot of the residual vector field on a 2D slice. The vectors are not randomly oriented but form coherent patterns, such as large-scale swirls and flows pointing from high-density regions to low-density regions. This strongly suggests the presence of a missing physical force in the hypothesized equation.

3.4 Quantitative inference and refinement of the momentum equation

The structured nature of the momentum residual R_V provides a clear path toward discovering the missing physics. Based on the principles of fluid dynam-

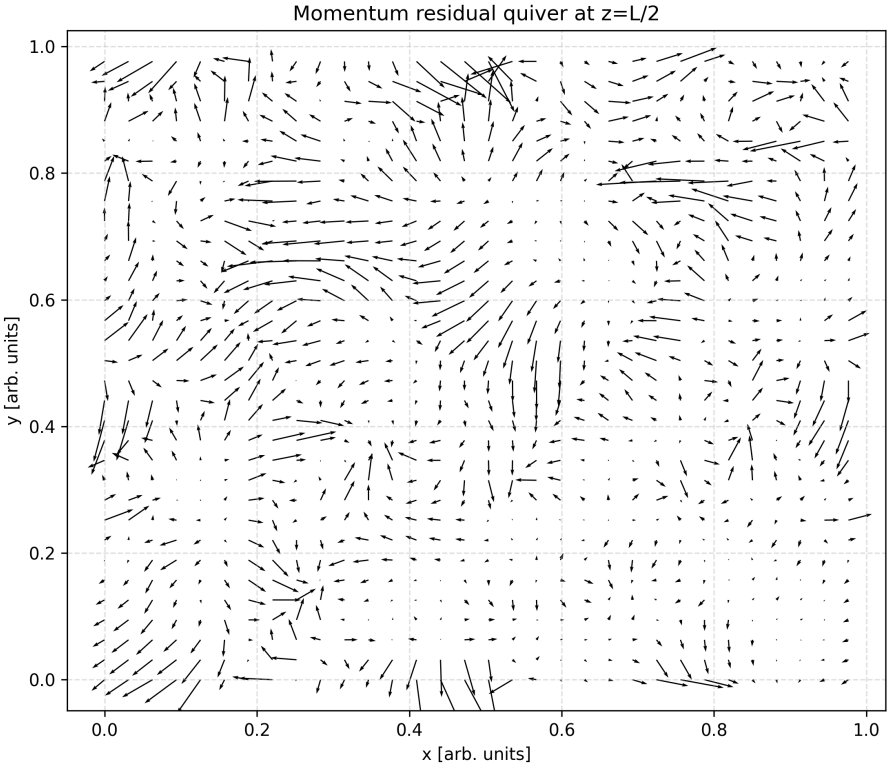

Figure 9: Quiver plot of the momentum residual vector field, R_V, on a 2D slice for the time interval $t = 4 \to 5$. The vectors show coherent, structured patterns, indicating a systematic missing force rather than random noise.

ics, two primary candidates for the missing force are the pressure gradient and viscous dissipation.

3.4.1 Pressure gradient force

The most common force in a fluid system is the pressure gradient, which acts to push fluid from high-pressure to low-pressure regions. The associated acceleration term is typically $-\frac{1}{\rho}\nabla P$. To test this hypothesis, a simple equation of state was assumed, where pressure is proportional to density, $P \propto \rho$. This is characteristic of an isothermal ideal gas. Under this assumption, the pressure gradient force term becomes proportional to $-\frac{1}{\rho}\nabla\rho$. This hypothesized force term, $F_P = -\frac{1}{\rho}\nabla\rho$, was computed for each time slice as described in the Methods.

To quantify the relationship between the momentum residual and this hypothesized force, the Pearson correlation coefficient was computed between the

components of R_V and F_P for the representative time slice $t = 4$. The results are presented in Table 2.

Table 2: Pearson Correlation Coefficients between Momentum Residual (R_V) and Hypothesized Force Terms at $t = 4$

Component	Correlation with $F_P = -\frac{1}{\rho}\nabla\rho$	Correlation with $F_\nu = \nabla^2\mathbf{v}$
x	0.610	0.140
y	0.641	0.142
z	0.606	0.143

The correlation coefficients between the residual and the pressure term are all strongly positive and significant, with values around 0.60-0.64. This indicates a moderately strong linear relationship. The scatter plots in the top row of Figure 10 visually confirm this correlation, showing a clear diagonal trend between the components of the residual and the components of the pressure force. This provides compelling evidence that a pressure gradient force is a major component of the missing physics.

3.4.2 Viscous force

Another candidate is a viscous force, which acts to dissipate kinetic energy and smooth out velocity gradients. For a Newtonian fluid, this is often modeled by a term proportional to the Laplacian of the velocity, $\nu\nabla^2\mathbf{v}$. This hypothesized viscous force, $F_\nu = \nabla^2\mathbf{v}$, was computed and correlated with the momentum residual, as detailed in the Methods.

As shown in Table 2, the Pearson correlation coefficients between the components of R_V and F_ν are very low, approximately 0.14 for all components. This indicates a very weak, almost negligible linear relationship. The corresponding scatter plots in the bottom row of Figure 10 show amorphous, cloud-like distributions, further confirming the lack of a simple linear relationship between the residual and the viscous term. This suggests that either viscosity is not a dominant force in this system, or it takes a more complex form than the simple Laplacian model.

3.5 Proposed governing equations

Based on the comprehensive validation and inference process, the spatio-temporal dynamics of the system are best described by the following set of partial differential equations:

1. **Continuity Equation (Mass Conservation):**

$$\frac{\partial\rho}{\partial t} + \nabla\cdot(\rho\mathbf{v}) = 0$$

This equation is strongly supported by the data, with residuals that are an order of magnitude smaller than the primary terms and can be reasonably attributed to numerical approximations, particularly the first-order temporal derivative.

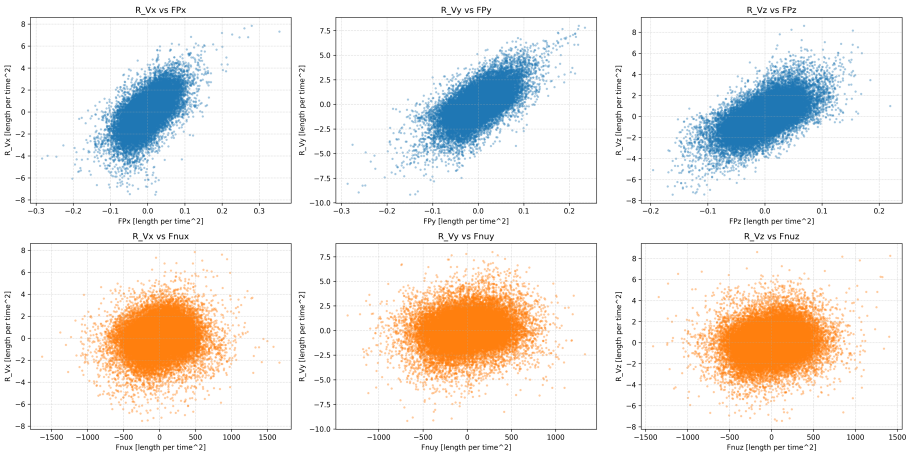

Figure 10: Scatter plots showing the correlation between the components of the momentum residual (R_V) and the hypothesized force terms (F_P and F_ν) for the time interval $t = 4 \to 5$. The top row shows a clear positive correlation with the pressure gradient term (F_P), while the bottom row shows negligible correlation with the viscous term (F_ν).

2. **Compressible Euler Equation (Momentum Conservation):**

$$\frac{\partial \mathbf{v}}{\partial t} + (\mathbf{v} \cdot \nabla)\mathbf{v} = -\frac{1}{\rho}\nabla P$$

The analysis provides overwhelming evidence for the necessity of both the advective term, $(\mathbf{v} \cdot \nabla)\mathbf{v}$, and a pressure gradient term, $-\frac{1}{\rho}\nabla P$. The strong correlation between the momentum residual and a pressure term derived from the assumption $P \propto \rho$ suggests that the system behaves like a compressible, inviscid fluid. While the assumption $P \propto \rho$ is a simplification, its strong correlation with the residual indicates that a pressure gradient is the dominant missing force. The contribution from a simple viscous term of the form $\nu\nabla^2\mathbf{v}$ appears to be negligible. In summary, the system is identified as being governed by the **compressible Euler equations**.

4 Conclusions

The discovery of fundamental spatio-temporal governing equations from observed system dynamics, particularly when temporal data is limited, presents a significant challenge in scientific inquiry. Traditional approaches often struggle with the inherent noise and inaccuracies in estimating temporal derivatives from sparse observations. This study addressed this challenge by introducing a novel constraint-based validation framework that rigorously evaluates candi-

date balance laws by leveraging robust spatial computations to constrain spatio-temporal dynamics.

Our methodology involved analyzing a dataset comprising ten time slices of density and velocity fields on a high-resolution 128^3 periodic spatial grid. Spatial derivatives were computed with high precision using spectral methods, while observed temporal changes were approximated via first-order finite differences. We then validated two candidate balance laws: the mass conservation (continuity) equation and a simplified momentum conservation law considering only advective acceleration. The core of our approach involved computing residuals between the observed temporal evolution and the evolution predicted solely from the robustly computed spatial terms. When significant, structured residuals were found, we employed correlation analysis to infer the nature of missing physical terms.

The results of our analysis provided clear insights into the system's governing equations. For mass conservation, the residuals between the observed temporal density change and the divergence of mass flux were consistently low across all time intervals, with an average Mean Absolute Error (MAE) of 0.035. This strong agreement indicates that the system's mass evolution is accurately described by the continuity equation. In contrast, a simplified momentum conservation law, which only accounted for advective acceleration, yielded significant and spatially structured residuals, with an average MAE of 1.717. This indicated that the simplified model was incomplete and a substantial missing force was at play.

Further quantitative analysis of these momentum residuals revealed a strong positive correlation (Pearson coefficients ranging from 0.60 to 0.64) with a hypothesized pressure gradient term, assuming pressure is proportional to density ($P \propto \rho$). Conversely, a simple viscous term (proportional to the Laplacian of velocity) showed negligible correlation (Pearson coefficients around 0.14).

From these findings, we have learned several key aspects about the system under investigation and the efficacy of our framework. Firstly, the constraint-based validation framework effectively identified the underlying physical laws even with limited temporal data, demonstrating its utility in scenarios where high-fidelity spatial data is available but temporal sampling is sparse. Secondly, the system rigorously adheres to the principle of mass conservation. Thirdly, the momentum dynamics are not solely driven by advection; a significant pressure gradient force is essential to accurately describe the system's acceleration. Finally, simple viscous effects appear to play a minor role in the observed dynamics. Collectively, these results lead to the conclusion that the spatio-temporal evolution of the system is accurately governed by the compressible Euler equations, which include both advection and a pressure gradient force, with viscous effects being minor.